The Kidney Model as an Inverse Problem

M. Breinbauer

Mathematische Analysen und Systeme GmbH (MAS)
Konrad-Adenauer-Allee 30
D-8400 Regensburg, West Germany

and

P. Lory

Mathematisches Institut
Technische Universität München
Postfach 20 24 20
D-8000 München 2, West Germany

Transmitted by Melvin R. Scott

ABSTRACT

The mammalian kidney is modeled by a multipoint boundary-value problem for a system of nonlinear ordinary differential equations. A corresponding inverse problem is presented, which allows the rigorous judgement of the potential of the given modeling technique. For its numerical solution a discretization is proposed, which is tailor-made for kidney models. It leads to a nonlinear-programming problem with nonlinear equality and inequality constraints. The suggested methods are applied to current research problems in renal physiology.

1. INTRODUCTION

During the last two decades mathematical kidney models of increasing complexity have become an indispensable tool in the effort towards a complete understanding of hypertonic urine formation. Hypotheses on the renal concentrating mechanism cannot be judged by purely experimental results. They must pass a test in the form of a mathematical simulation based on principles of local mass balance. In the case of steady-state simulations,

these principles lead to a boundary-value problem for a system of nonlinear ordinary differential equations.

Naturally, this boundary-value problem depends on many geometric and thermodynamic parameters, like solute permeabilities of the membranes in the various tubular segments. Because of their biological nature, most of these data can be measured only with considerable uncertainty.

A completely satisfactory kidney model must meet two requirements: First, it must use parameters within their ranges of measurements. Second, the model must predict steep concentration gradients in the inner medulla in accord with tissue-slice experiments. This requirement is the bottleneck for present-day kidney models [1]. As a consequence, it is absolutely essential to know which values of the parameters (within their ranges of uncertainty) predict the strongest increase of inner medullary concentration. This is the inverse problem, which is studied in the present paper. Commonly this task has been attacked by a mixture of heuristic arguments and trial-and-error strategies.

The present paper suggests a more systematic approach: The boundary-value problem is discretized in a semidiscrete manner. Thus, the original inverse problem is reduced to a nonlinear optimization problem with 100 independent variables, 84 nonlinear equality constraints, and 38 inequality constraints. This can be solved effectively by the sequential quadratic programming method.

Besides the physiological insights that can be gained by this approach, the arising nonlinear optimization problem may also be of interest as a test problem for optimization software.

The paper is structured as follows: The boundary-value problem modeling the kidney is formulated in Section 2. The inverse problem and its numerical solution are presented in Section 3. Section 4 applies these techniques to current research in renal physiology. The consequences of these results are commented in the concluding remarks of Section 5.

2. THE BOUNDARY-VALUE PROBLEM MODELING THE RENAL CONCENTRATING MECHANISM

The mammalian kidney consists of thousands of similar functional units, called nephrons. A schematic diagram of a single nephron forming a counter-current system is given in Figure 1. Fluid flows in sequence through the descending and the ascending limb of Henle's loop (DLH and ALH), the distal tubule (DT), and the collecting duct (CD). At its end the fluid emerges into the pelvis. All the nephrons are embedded in a common compartment, called the central core (CC; see [2, 3]).
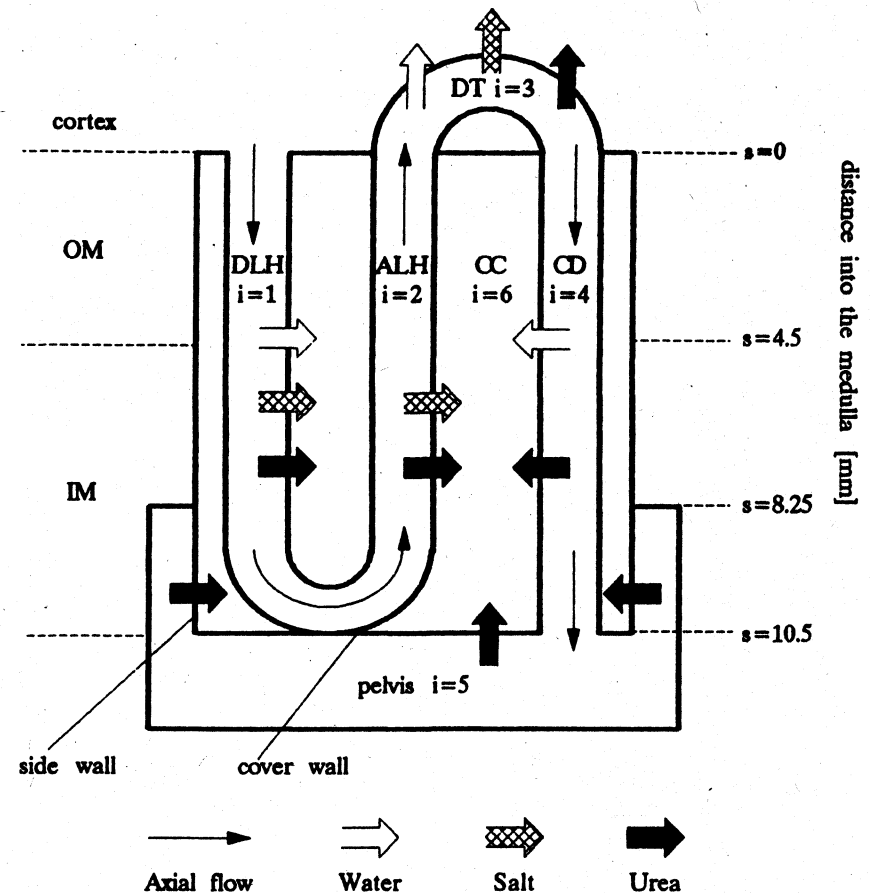

FIG. 1. Schematic diagram of a single long nephron. The indicated orientations of the arrows correspond to positive fluxes. DLH (ALH), descending (ascending) limb of Henle's loop; DT, distal tubule; CD, collecting duct; CC, central core; OM (IM), outer (inner) medulla.

Two solutes are present in the model: salt ($l = 1$) and urea ($l = 2$). Exchange between the nephron segments occurs through solute and water movement in the central core. The diagram reflects the impermeability of the ALH to water and the impermeability of the CD to salt (cf. the discussion in [4]). In addition, Figure 1 defines a numbering of the various segments.

The loops of Henle extend to varying depths within the renal medulla. In order to model the architecture of this tubular system (which is described in [5]), the inner medulla is subdivided into three parts (Figure 2). The number
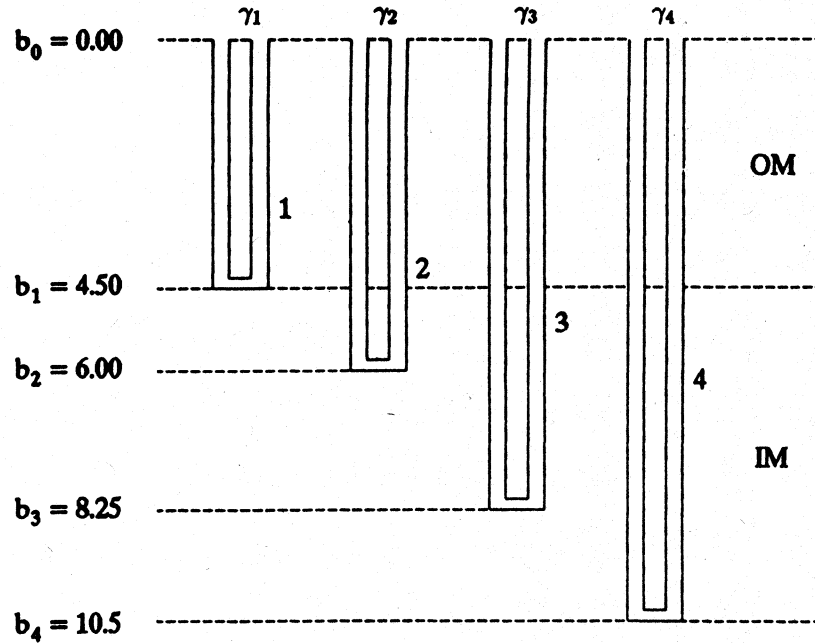
FIG. 2.   Distribution of the 1536 loops of Henle. OM (IM), outer (inner) medulla.

of loops of length b_j is given by γ_j. Altogether, 1536 loops are present in the model. This number is chosen because 1536 loops eventually merge into one CD. As a consequence,

$$\gamma_1 + \gamma_2 + \gamma_3 + \gamma_4 = 1536. \tag{1}$$

The following paragraph describes the modeling of the DLH of length b_j: Let F_{1v}^j and F_{1l}^j denote the axial volume flow rate and the axial flow rate of solute l in this tubular segment, r_1 its radius, and s the distance into the medulla from the corticomedullary border. The following system of differential equations results from the requirement of local mass balance:

$$\frac{dF_{1v}^j}{ds} = -2\pi r_1 \cdot J_{1v}^j, \qquad j = 1,\ldots,4, \tag{2}$$

$$\frac{dF_{1l}^j}{ds} = -2\pi r_1 \cdot J_{1l}^j, \qquad l = 1,2, \quad j = 1,\ldots,4. \tag{3}$$

According to the laws of irreversible thermodynamics (see [6]) the transmural fluxes are given by

$$J_{1v}^j = \mathrm{Lp}_1\left[1.82\sigma_{11}\big(C_{61} - C_{11}^j\big) + \sigma_{12}\big(C_{62} - C_{12}^j\big)\right] \tag{4}$$

$$J_{1l}^j = P_{1l} \cdot \big(C_{1l}^j - C_{6l}\big) + (1 - \sigma_{1l})J_{1v}^j \overline{C}_{1l}^j, \tag{5}$$

where $\overline{C}_{1l}^j := (C_{1l}^j + C_{6l})/2$. The concentration of solute l in the DLH of length b_j is given by

$$C_{1l}^j = F_{1l}^j / F_{1v}^j, \qquad l = 1,2, \quad j = 1,\ldots,4. \tag{6}$$

It is assumed that axial movement in the tubules is dominated by convection; thus diffusive flow is neglected in Equation (6). Physiological arguments in [7] and comparative computations in [8] justify this simplification.

Further details of the notation may be found in the glossary of symbols in Table 1. Note that Equations (2)–(6) are not self-contained, because they are coupled with other equations (which will be given below) via the CC concentrations C_{6l}.

The ascending limbs of Henle's loop are impermeable to water [9, 10], and the ALH system is modeled by

$$\frac{dF_{2v}^j}{ds} = 0, \qquad j = 1,\ldots,4, \tag{7}$$

$$\frac{dF_{2l}^j}{ds} = -2\pi r_2 \cdot J_{2l}^j, \qquad l = 1,2, \quad j = 1,\ldots,4. \tag{8}$$

The transmural fluxes are given by

$$J_{2l}^j = P_{2l} \cdot \big(C_{2l}^j - C_{6l}\big) + T_{2l}^j, \qquad C_{2l}^j = F_{2l}^j / F_{2v}^j. \tag{9}$$

The active transport T_{2l}^j is assumed to obey Michaelis-Menten kinetics, namely

$$T_{2l}^j = \frac{\mathrm{Vm}_{2l} C_{2l}^j}{\mathrm{Km}_{2l} + C_{2l}^j}, \tag{10}$$

where Vm_{2l} is the maximum rate of transport, and Km_{2l} is the Michaelis constant. In the model, only salt is transported actively (i.e. $T_{22} = 0$), and this

TABLE 1
GLOSSARY OF SYMBOLS [a]

b_j	Lengths of loops of Henle (see Figure 2) [mm]
γ_j	Number of loops of length b_j
s	Distance into the medulla from the corticomedullary border ($s = 0$) to the papillary tip ($s = 10.5$); independent variable (see Figure 1)[b] [mm]
F_{iv}^j	Axial volume flow rate in the DLH ($i = 1$) and in the ALH ($i = 2$) of length b_j [nl/min]
F_{il}^j	Axial flow rate of solute l in the DLH ($i = 1$) and in the ALH ($i = 2$) of length b_j [10^{-9} mmol/min]
r_i	Radius of tube i [mm]
J_{1l}^j	Transmural flux out of the DLH of length b_j [nl min^{-1} mm^{-2}]
J_{il}^j	Transmural flux of solute l out of the DLH ($i = 1$) and out of the ALH ($i = 2$) of length b_j [10^{-9} mmol min^{-1} mm^{-2}]
C_{il}^j	Concentration of solute l in the DLH ($i = 1$) and in the ALH ($i = 2$) of length b_j [mmol/l]
C_{il}	Concentration of solute l in the DT ($i = 3$), in the CD ($i = 4$), in the pelvis ($i = 5$), and in the CC ($i = 6$) [mmol/l]
Lp_i	Hydraulic water conductivity of the wall of segment i [nl mm^{-2} min^{-1} (mosmol/l)$^{-1}$]
σ_{il}	Reflection coefficient of the wall of segment i for solute l
P_{il}	Permeability of the wall of segment i for solute l [10^{-3} mm/min]
T_{i1}	Active salt transport out of the ALH ($i = 2$) and out of the DT ($i = 3$) [10^{-9} mmol min^{-1} mm^{-2}]
Vm_{i1}	Maximum rate of the active salt transport out of the ALH ($i = 2$) and out of the DT ($i = 3$) [10^{-9} mmol min^{-1} mm^{-2}]
Km_{i1}	Michaelis constant of the active salt transport out of the ALH ($i = 2$) and out of the DT ($i = 3$) [mmol/l]
$\mathscr{F}_{iv}$	Axial volume flow rate in the composite structure for the distal tubules ($i = 3$) and for the collecting ducts ($i = 4$); see text [nl/min]
$\mathscr{F}_{il}$	Axial flow rate of solute l in the composite structure for the distal tubules ($i = 3$) and for the collecting ducts ($i = 4$); see text [10^{-9} mmol/min]
J_{iv}	Transmural water flux out of the DT ($i = 3$) and out of the CD ($i = 4$) [nl min^{-1} mm^{-2}]
J_{il}	Tranmsural flux of solute l out of the DT ($i = 3$), out of the CD ($i = 4$), and out of the pelvis ($i = 5$) [10^{-9} mmol min^{-1} mm^{-2}]
Cp_l	Concentration of solute l in the plasma [mmol/l]
$NCD(s)$	Number of collecting ducts present at depth s of the medulla
PRUS	Pelvic reflux of urea across the side wall of the CC (see Figure 1) [10^{-9} mmol/min]
$CF_5(s)$	Circumference of the total medulla $\times$ 1536/(total number of loops of a kidney) [mm]
D_l	Diffusion coefficient of solute l [10^{-3} mm^2/min]
$AC(s)$	Cross-sectional area of the CC [mm^2]
F_{6v}	Axial volume flow rate in the CC [nl/min]
F_{6l}	Axial flow rate of solute l in the CC [10^{-9} mmol/min]

TABLE 1 (*Continued*)

Q_0	Volume flow rate entering the DLH [nl/min]
L_{DT}	Length of distal tubule [mm]
PRUC	Pelvic reflux of urea across the cover wall of the CC (see Figure 1) [10^{-9} mmol/min]

[a] In the order in which they appear in Equations (1)–(34).

[b] For $i = 3$, s is measured along the distal tubule. DLH (ALH), descending (ascending) limb of Henle's loop; DT, distal tubule; CD, collecting duct; CC, central core.

transport occurs only in the outer medullary section of the ALH and in the distal tubule (passive mode [2, 11]).

The distal tubules are modeled by a composite structure (cf. [7]). The flows $\mathscr{F}_{3v}$, $\mathscr{F}_{3l}$ of the composite structure represent the sums of flows in the single tubules, and the concentrations

$$C_{3l} = \mathscr{F}_{3l} / \mathscr{F}_{3v} \tag{11}$$

of the fluid within the composite structure reflect the mixture of the fluids in the single tubules. The 1536 distal tubules are modeled by

$$\frac{d\mathscr{F}_{3v}}{ds} = -2\pi r_3 \times 1536 J_{3v}, \tag{12}$$

$$\frac{d\mathscr{F}_{3l}}{ds} = -2\pi r_3 \times 1536 J_{3l}, \qquad l = 1, 2. \tag{13}$$

Here, s is measured along the distal tubules from $s = 0$ to $s = L_{DT}$. During this passage, the fluid interacts with the cortical interstitium, where the solute concentrations are assumed to be the same as in the arterial plasma, namely Cp_1 and Cp_2. Consequently,

$$J_{3v} = Lp_3 \left[1.82\sigma_{31}(Cp_1 - C_{31}) + \sigma_{32}(Cp_2 - C_{32}) \right], \tag{14}$$

$$J_{3l} = P_{3l} \cdot (C_{3l} - Cp_l) + (1 - \sigma_{3l}) J_{3v} \overline{C}_{3l} + T_{3l}, \qquad l = 1, 2, \tag{15}$$

where $\overline{C}_{3l} := (C_{3l} + Cp_l)/2$. Again, only salt is transported actively (i.e. $T_{32} = 0$), and this active transport T_{31} obeys Michaelis-Menten kinetics.

The geometry of the collecting duct system is described in [5]: Six nephrons drain into one collecting duct. Their number remains constant in the outer medulla. In the inner medulla, the collecting ducts merge in a dichotomous manner on eight successive levels. Consequently, the number of collecting ducts present at depth s of the medulla is modeled by the function

$$NCD(s) = \begin{cases} 256 & \text{for } 0 \leqslant s < 4.5 \\ 128 \exp[-0.80867(s-4.5)] & \text{for } 4.5 \leqslant s \leqslant 10.5. \end{cases}$$

Note that $NCD(10.5) = 1$. Similarly to the distal tubules, the collecting-duct system is modeled by a composite structure:

$$\frac{d\mathscr{F}_{4v}}{ds} = -2\pi r_4 \cdot NCD(s) \cdot J_{4v}, \tag{16}$$

$$\frac{d\mathscr{F}_{4l}}{ds} = -2\pi r_4 \cdot NCD(s) \cdot J_{4l}, \quad l = 1,2, \tag{17}$$

where

$$J_{4v} = Lp_4 [1.82\sigma_{41}(C_{61} - C_{41}) + \sigma_{42}(C_{62} - C_{42})], \tag{18}$$

$$J_{4l} = P_{4l} \cdot (C_{4l} - C_{6l}) + (1 - \sigma_{4l}) J_{4v} \overline{C}_{4l}, \tag{19}$$

$$C_{4l} = \frac{\mathscr{F}_{4l}}{\mathscr{F}_{4v}}, \qquad \overline{C}_{4l} = \frac{C_{4l} + C_{6l}}{2}. \tag{20}$$

The transmural flux of urea across the side wall of the CC is given by

$$J_{52} = P_{52} \cdot (C_{52} - C_{62}), \tag{21}$$

and the corresponding pelvic reflux amounts to

$$PRUS = \int_{8.25}^{10.5} CF_5(s) J_{52}(s) \, ds.$$

This equation allows a trivial transformation to the differential equation

$$prus'(s) = CF_5(s) J_{52}(s). \tag{22}$$

If $prus(8.25) = 0$, then $PRUS = prus(10.5)$.

The differential equations (2)–(10), (16)–(22) are coupled by the CC concentrations C_{6l}, which obey the central-core equations

$$F_{6l} = F_{6v} C_{6l} - D_l AC(s) \frac{dC_{6l}}{ds}, \quad l = 1,2, \tag{23}$$

where D_l is the diffusion coefficient of solute l, and $AC(s)$ denotes the cross-sectional area of the CC. Equation (23) allows solute movement along the CC axis by both diffusion and convection. The central-core flows F_{6v}, F_{6l} obey the following differential equations, which are derived from the requirement of mass balance:

$$\frac{dF_{6v}}{ds} = \sum_{j=j_a}^{4} \gamma_j 2\pi r_1 J_{1v}^j + 2\pi r_4 NCD(s) J_{4v}, \tag{24}$$

$$\frac{dF_{6l}}{ds} = \sum_{j=j_a}^{4} \gamma_j (2\pi r_1 J_{1l}^j + 2\pi r_2 J_{2l}^j)$$

$$+ 2\pi r_4 NCD(s) J_{4l} + CF_5(s) J_{5l}, \quad l = 1,2, \tag{25}$$

where $J_{51} \equiv 0$ for $s \in [0,10.5]$, $J_{52} \equiv 0$ for $s \in [0,8.25]$, and $j_a = v$ for $s \in [b_{v-1}, b_v]$ ($v = 1, \ldots, 4$).

The boundary conditions for the system of differential equations (2)–(25) are given by

$$F_{1v}^j(0) = Q_0, \qquad j = 1, \ldots, 4,$$

$$F_{11}^j(0) = Q_0 Cp_1, \qquad j = 1, \ldots, 4, \tag{26}$$

$$F_{12}^j(0) = Q_0 \times 2 Cp_2, \qquad j = 1, \ldots, 4;$$

$$F_{2v}^j(b_j) = -F_{1v}^j(b_j), \qquad j = 1, \ldots, 4,$$

$$F_{2l}^j(b_j) = -F_{1l}^j(b_j), \qquad j = 1, \ldots, 4, \quad l = 1,2; \tag{27}$$

$$\mathscr{F}_{3v}(0) = -\sum_{j=1}^{4} \gamma_j F_{2v}^j(0), \qquad \mathscr{F}_{3l}(0) = -\sum_{j=1}^{4} \gamma_j F_{2l}^j(0), \quad l = 1,2; \tag{28}$$

$$\mathscr{F}_{4v}(0) = \mathscr{F}_{3v}(L_{DT}), \qquad \mathscr{F}_{4l}(0) = \mathscr{F}_{3l}(L_{DT}), \quad l = 1,2; \tag{29}$$

$$prus(8.25) = 0; \tag{30}$$

$$\mathscr{F}_{42}(10.5) = \mathscr{F}_{4v}(10.5) \cdot C_{52} + PRUS + PRUC; \tag{31}$$

$$C_{6l}(0) = Cp_l, \quad l = 1,2; \tag{32}$$

$$F_{6v}(10.5) = F_{61}(10.5) = 0, \qquad F_{62}(10.5) = -PRUC, \tag{33}$$

where PRUC denotes the pelvic urea reflux across the cover wall of the CC. It

is given by

$$\text{PRUC} = \text{AC}(10.5) \cdot P_{52}[C_{52} - C_{62}(10.5)]. \qquad (34)$$

At the beginning of each tubule, the axial rate of flow of each constituent is fixed by the boundary conditions (26). The boundary conditions (27)–(29) serve to connect the ends of the descending limbs to the beginnings of the ascending limbs, the ends of the ascending limbs to the beginnings of the distal tubules, and the ends of the distal tubules to the beginnings of the collecting ducts. The boundary condition (31) results from the requirement of mass balance in the pelvis.

Equations (2)–(34) define a boundary-value problem for a system of 36 simultaneous nonlinear differential equations of first order with the unknown functions $F_{1v}^j, F_{1l}^j, F_{2v}^j, F_{2l}^j, \mathscr{F}_{3v}, \mathscr{F}_{3l}, \mathscr{F}_{4v}, \mathscr{F}_{4l}$, prus, C_{6l}, F_{6v}, F_{6l} ($l = 1, 2$; $j = 1, \ldots, 4$) and the unknown constant C_{52} (eigenvalue problem). The geometric and thermodynamic parameters will be given in Section 4.

REMARK 2.1. In the simulations of Section 4, the four descending limbs have different lengths b_j, but apart from that, their parameters are identical. Consequently, the model (2)–(34) is equivalent to a model with a single descending limb. The index j in Equations (2)–(6), (26), in the transmural DLH fluxes of (24), (25), and in the DLH flows of (27) can be dropped. Thus the number of differential equations can be reduced to 27.

REMARK 2.2. The systems modeling technique used in this section has been employed previously by several authors to study various aspects of the integrated renal function [1, 4, 7, 8, 12–20]. Finite-difference methods [12–14, 16, 20–23], quasilinearization [1, 24–27], invariant imbedding [27–31], and multiple shooting [4, 17, 32] have been suggested for the numerical solution of the resulting boundary-value problems. A semidiscrete method combining collocation and shooting has been given in [19, 33]. The classical theoretical results on the orders of convergence for pure collocation [34] extend to this semidiscrete modification.

3. THE INVERSE PROBLEM AND ITS NUMERICAL SOLUTION

The differential equations and boundary conditions of Section 2 constitute a multipoint boundary-value problem

$$z' = \Phi(s, z; p), \qquad (35)$$

$$\beta(z(b_0; p), \ldots, z(b_4; p); p) = 0, \qquad (36)$$

where p denotes a vector of parameters which are of thermodynamic and geometric nature. The values of these parameters can be determined only by difficult and time-consuming experimental techniques, and they are known only with considerable uncertainty. In the inverse approach of the present paper, they are allowed to vary within certain intervals, i.e.

$$l \leqslant p \leqslant u, \qquad (37)$$

where l and u denote vectors of lower and upper bounds respectively. These intervals reflect the corresponding ranges of measurements. It has already been pointed out in Section 1 that a judgment of a given kidney model requires the knowledge of the optimal inner medullary concentration increase which can be generated by this model. So the objective function is given by

$$\underset{p}{\text{maximize}} \left[\text{Osm}_6(10.5; p) - \text{Osm}_6(4.5; p)\right], \qquad (38)$$

where

$$\text{Osm}_i(s; p) := 1.82 C_{i1}(s; p) + C_{i2}(s; p) \qquad (39)$$

denotes the total osmolarity in compartment i. In addition to (37), further constraints are imposed on the parameters: First, experimental results [35] demonstrate that the osmolarity of the collecting duct fluid at the papillary tip is nearly the same as that of the fluid in the adjacent central core at the same level. This fact is modeled by the constraint

$$0.9\,\text{Osm}_4(10.5; p) \leqslant \text{Osm}_6(10.5; p) \leqslant 1.1\,\text{Osm}_4(10.5; p). \qquad (40)$$

Second, the volume flow rate emerging from the final collecting duct into the pelvis exceeds a certain bound [36]:

$$\text{TF/P inulin CD}(10.5; p) \leqslant 400, \qquad (41)$$

where

$$\text{TF/P inulin CD}(s; p) := \frac{3 \times 1536 Q_0}{\mathscr{F}_{4v}(s; p)} \qquad (42)$$

denotes the simulated tubule-fluid-to-plasma ratio for the inulin concentra-

tion in the collecting duct at level s. Third, the salt concentration at the outer-inner medullary junction of the central core is within certain bounds [37]:

$$350 \leqslant C_{61}(4.5; p) \leqslant 500. \tag{43}$$

The numerical solution of the inverse problem (35)–(43) follows the semidiscrete approach given in [33]: It makes use of the sparsity of the system (35) by exploiting the fact that the tubule equations are connected only via the central-core concentrations C_{6l}. The method is based on splines as trial functions for these concentrations and on collocation of the central-core equations (23). Once these trial functions are given, the tubule equations and boundary conditions form a sequence of initial-value problems (each in the corresponding direction of flow). These initial-value problems are very stable.

The definition of the trial functions (splines) $C_{\Delta,61}$ and $C_{\Delta,62}$ requires the selection of a partition $\Delta = (s_j)_{j=0}^N$ of the interval $[0.0, 10.5]$,

$$\Delta: \quad 0.0 = s_0 < s_1 < s_2 < \cdots < s_N = 10.5, \tag{44}$$

which has to include the points b_1, b_2, b_3 where the right-hand side Φ of Equation (35) is discontinuous. For an adaptive placement of the partition points s_j, an adequately modified version of the code NEWNOT [38] is effective. The space of trial functions is given by

$$\Pi_{k,\Delta} \cap C[0.0, 10.5],$$

where $\Pi_{k,\Delta}$ denotes the linear space of piecewise polynomials of degree $\leqslant k$ with partition points Δ. A reasonable choice is $k = 3$.

Normalized B-splines (cf. [38]) are used as basis functions. Let

$$C_{\Delta,6l} = \sum_{j=1}^{kN+1} \alpha_{jl} B_{j,k+1}, \quad l = 1,2 \tag{45}$$

be the B-representations for the trial functions. Because of the boundary conditions (32), $\alpha_{1l} = Cp_l$. So the $2kN$-dimensional vector

$$\alpha := (\alpha_{21}, \ldots, \alpha_{kN+1,1}, \alpha_{22}, \ldots, \alpha_{kN+1,2}) \tag{46}$$

has to be determined such that $C_{\Delta,6l}$ approximate C_{6l} ($l = 1,2$). For that

purpose collocation is applied to the central-core equations (23): Let σ_i ($i = 1, \ldots, kN$) denote the Gauss-Legendre collocation points (k per subinterval of the partition Δ, and distributed the same in each subinterval; see e.g. [38]). The trial functions are forced to exactly satisfy the differential equations (23) at these points, i.e.

$$\mathrm{fc}_{il}(\alpha, p) = 0, \tag{47}$$

where

$$\mathrm{fc}_{il}(\alpha, p) := C'_{\Delta,6l}(\sigma_i; \alpha) - \frac{F_{\Delta,6v}(\sigma_i; \alpha, p)C_{\Delta,6l}(\sigma_i; \alpha) - F_{\Delta,6l}(\sigma_i; \alpha, p)}{D_l \cdot \mathrm{AC}(\sigma_i; p)} = 0,$$

$$i = 1, \ldots, kN, \quad l = 1,2.$$

Here, $F_{\Delta,6v}$ and $F_{\Delta,6l}$ together with $F_{\Delta,1v}, F_{\Delta,1l}, F_{\Delta,2v}^j, F_{\Delta,2l}^j, \mathscr{F}_{\Delta,3v}, \mathscr{F}_{\Delta,3l}$, $\mathscr{F}_{\Delta,4v}, \mathscr{F}_{\Delta,4l}, \mathrm{prus}_\Delta, C_{\Delta,52}$ denote the solution of the differential equations (2)–(22), (24), (25) subject to the boundary conditions (26)–(31), (33), (34), where the concentrations C_{6l} in the right-hand sides of the differential equations and in (34) are replaced by the trial functions $C_{\Delta,6l}$ ($l = 1,2$). Note that according to Remark 2.1 the index j in the DLH flows can be dropped.

Owing to the typical connectivity of the system of the nephrons, the above functions can be computed efficiently in a natural and straightforward manner: The initial-value problems (2)–(6), (26) for the DLH; (7)–(10), (27) for the ALH; (11)–(15), (28) for the DT; (16)–(20), (29) for the CD are computed in sequence. For these integrations, routines are used that control the discretization error reliably, namely the programs DIFSY1 (Bulirsch-Gragg-Stoer extrapolation method [39–41]), RKF7 (Runge-Kutta-Fehlberg method of order 7 [42]), and DGEAR (backward differentiation formulas (43]). Note that these integrations always take place in the stable direction of tubular flow. At its end, the values of the functions $F_{\Delta,1v}, F_{\Delta,1l}, F_{\Delta,2v}^j, F_{\Delta,2l}^j$, $\mathscr{F}_{\Delta,4v}, \mathscr{F}_{\Delta,4l}$ at the collocation points and at the endpoints of the interval $[0.0, 10.5]$ are available.

Equations (21), (22), (31), (34) can be combined to

$$\mathscr{F}_{\Delta,42}(10.5; \alpha, p)$$
$$= C_{\Delta,52}(\alpha, p)$$
$$\times \left[\mathscr{F}_{\Delta,4v}(10.5; \alpha, p) + P_{52} \cdot \left(\int_{8.25}^{10.5} \mathrm{CF}_5(s; p)\, ds + \mathrm{AC}(10.5; p) \right) \right]$$
$$- P_{52} \cdot \left(\int_{8.25}^{10.5} \mathrm{CF}_5(s; p)C_{\Delta,62}(s; \alpha)\, ds + \mathrm{AC}(10.5; p)C_{\Delta,62}(10.5; \alpha) \right),$$

and the constant $C_{\Delta,52}(\alpha, p)$ can be easily computed from this equation.

The computation of the functions fc_{il} is completed by integrating the differential equations (3), (8), (17), (25) from $s = 10.5$ to $s = \sigma_i$. This together with the boundary conditions (27), (33) yields (e.g. for $l = 2$)

$$F_{\Delta,62}(\sigma_i; \alpha, p) = - \sum_{j=j_a}^{4} \gamma_j \left[F_{\Delta,12}(\sigma_i; \alpha, p) + F_{\Delta,22}^j(\sigma_i; \alpha, p) \right]$$

$$- \mathscr{F}_{\Delta,42}(\sigma_i; \alpha, p) - \int_{\sigma_i}^{10.5} CF_5(s; p) J_{\Delta,52}(s; \alpha, p)\, ds$$

$$+ \mathscr{F}_{\Delta,42}(10.5; \alpha, p) - \text{PRUC}.$$

This equation describes the conservation of mass over the $[\sigma_i, 10.5]$ section of the medulla. It allows the straightforward calculation of $F_{\Delta,62}(\sigma_i; \alpha, p)$. The values $F_{\Delta,6v}(\sigma_i; \alpha, p)$ and $F_{\Delta,61}(\sigma_i; \alpha, p)$ can be computed analogously. Hence, the functions fc_{il} [cf. the definition (47)] can be evaluated in a stable and efficient manner.

Let m be that index for which $s_m = 4.5$ in the partition (44). Then the (discrete) *nonlinear-programming problem* which approximates the inverse problem (35)–(43) can be formulated:

$$\text{maximize } 1.82(\alpha_{kN+1,1} - \alpha_{km+1,1}) + (\alpha_{kN+1,2} - \alpha_{km+1,2}), \quad (48)$$

where the independent variables (α, p) are subject to

nonlinear equality constraints:

$$fc_{il}(\alpha, p) = 0 \quad (i = 1,\dots,kN, \quad l = 1,2); \quad (49)$$

nonlinear inequality constraints:

$$0.9 \frac{1.82 \mathscr{F}_{\Delta,41}(10.5; \alpha, p) + \mathscr{F}_{\Delta,42}(10.5; \alpha, p)}{\mathscr{F}_{\Delta,4v}(10.5; \alpha, p)}$$

$$\leqslant 1.82 \alpha_{kN+1,1} + \alpha_{kN+1,2}$$

$$\leqslant 1.1 \frac{1.82 \mathscr{F}_{\Delta,41}(10.5; \alpha, p) + \mathscr{F}_{\Delta,42}(10.5; \alpha, p)}{\mathscr{F}_{\Delta,4v}(10.5; \alpha, p)}, \quad (50)$$

$$10 \leqslant \frac{3 \times 1536 Q_0}{\mathscr{F}_{\Delta,4v}(10.5; \alpha, p)} \leqslant 400; \quad (51)$$

bounds:

$$350 \leqslant \alpha_{km+1,1} \leqslant 500, \quad (52)$$

$$l \leqslant p \leqslant u. \quad (53)$$

Note that $\alpha_{kN+1,l} = C_{\Delta,6l}(10.5; \alpha, p)$ and $\alpha_{km+1,l} = C_{\Delta,6l}(4.5; \alpha, p)$. Hence, the objective function (48) is an approximation of the original objective function (38). The equality constraints (49) are the collocation conditions (47). The inequalities (50) and the right inequality of (51) reflect the constraints (40) and (41) of the original problem. Note also that the flows $\mathscr{F}_{\Delta,4v}(10.5; \alpha, p)$ and $\mathscr{F}_{\Delta,4l}(10.5; \alpha, p)$ are computed as a by-product during the evaluation of the functions $fc_{il}(\alpha, p)$. The left inequality of (51) avoids calculations in a physiologically meaningless range. The bounds (52) and (53) correspond to (43) and (37) respectively.

For the numerical solution of the nonlinear programming problem (48)–(53) canned software is available. The package SLSQP [44] has been used for the computations in Section 4. It implements the *sequential quadratic-programming method* algorithm as developed in [45–50]. This technique is also referred to as Lagrange-Newton or SOLVER method [51]. Extensive tests in [52] on a wide range of test examples [53] have demonstrated its excellent efficiency in terms of function evaluations. This is a decisive feature because the evaluation of the constraint functions (49)–(51) is a rather time-consuming task.

In particular, SLSQP uses the exact L1 penalty function of [46] as a test function within the steplength algorithm. The matrices approximating the Hessian matrix of the Lagrangian function are updated by the BFGS formula of [47, 48]. The quadratic-programming subproblems are transformed to linear least-squares problems [50], which are solved by the software of [54].

4. SIMULATIONS AND RESULTS

The techniques of Sections 2 and 3 have been applied during several simulations studying current research problems of renal physiology in [55]. The present section gives a small selection of these results.

Table 2 lists those thermodynamic parameters which are held fixed during the computations. They are discussed and justified in [4, 19]. As far as possible values are those measured directly in isolated perfused tubules of the rabbit. In addition, $Q_0 = 10$ nl/min, $Cp_1 = 140$ mmol/l, $Cp_2 = 9$ mmol/l, $Km_{21} = Km_{31} = 100$ mmol/l. The radii of the individual tubes are: $r_1 = 8$ μm, $r_2 = 10$ μm, $r_4 = 12$ μm in the outer medulla, $r_4 = 24$ μm in the inner

TABLE 2

FIXED THERMODYNAMIC PARAMETERS [a]

	ALH			CD	
	OM	IM	DT	OM	IM
Lp, $nl\,cm^{-2}\,min^{-1}$ $\times(mosmol/l)^{-1}$	0	0	48.4	Var.[b]	Var.[b]
P_{salt}, 10^{-5} cm/s	6.27	25	0.8	0	0
P_{urea}, 10^{-5} cm/s	0	6.7	Lin. trans.[c]	0.097	Var.[b]
σ_{salt}	—	—	1	1	1
σ_{urea}	—	—	1	Var.[b]	Var.[b]

[a] ALH, ascending limb of Henle's loop; Dt, distal tubule; CD, collecting duct; OM, outer medulla; IM, inner medulla; Lp, hydraulic water conductivity; P_{salt}, permeability to salt; P_{urea}, permeability to urea; σ_{salt}, reflection coefficient for salt; σ_{urea}, reflection coefficient for urea.

[b] Variable; see Table 3.

[c] Linear transition from 0 to 1.

medulla. The radius r_3 decreases linearly from 10 to 8 μm. The length of the distal tubule is $L_{DT} = 2.625$ mm. The cross-sectional area $AC(s)$ of the central core and the circumference of the total medulla are chosen analogously to [4].

The other parameters are allowed to vary over certain intervals. These parameters constitute the vector p of Section 3. The corresponding lower and upper bounds are given in Table 3. The chosen upper bounds for the maximum rates of active salt transport, Vm_{i1}, are relatively large in order to allow high flexibility. Note that in the results given below the computed optima for Vm_{i1} are much lower than these upper bounds. The intervals for the DLH parameters cover the various modes that have been studied in [7]. The intervals for the CD parameters reflect the ranges of measurements. Cf. [4, 7, 18, 19] (together with the references cited there) and the recent results of [56]. Again, most of these measurements are in rabbits. The consequences of various permeabilities for the reentry of pelvic urea into the papillary central core have been studied in [4] (but see the discussion below). The lower bound for the parameter ρ_1 ensures that at least two-thirds of the loops are short loops [5]. However, no further restrictions are imposed on the loop geometry (within the frame inherent in the selection of four groups of loops with lengths $b_1,\ldots,b_4$ in Figure 2, of course). In the following, the above parameter set will be referred to as the base case. The bounds of Table 3 define the vectors l and u of the inequalities (37). The objective function (38) and the constraints (40)–(43) complete the definition of the inverse problem.

TABLE 3

BOUNDS FOR VARIABLE PARAMETERS

Parameter	Lower bound	Upper bound
Maximum rates of active transport		
Vm_{21}, 10^{-6} $mmol\,cm^{-2}\,s^{-1}$	0	44
Vm_{31}, 10^{-6} $mmol\,cm^{-2}\,s^{-1}$	0	44
Descending limb of Henle's loop		
Lp_1, $nl\,cm^{-2}\,min^{-1}(mosmol/l)^{-1}$	5	252
P_{11}, 10^{-5} cm/s	0	47
P_{12}, 10^{-5} cm/s	0	20
σ_{11}	0.36	1
σ_{12}	0.4	1
Outer medullary collecting duct		
Lp_4, $nl\,cm^{-2}\,min^{-1}(mosmol/l)^{-1}$	23	48.4
σ_{42}	0.4	1
Inner medullary collecting duct		
Lp_4, $nl\,cm^{-2}\,min^{-1}(mosmol/l)^{-1}$	7.37	92
P_{42}, 10^{-5} cm/s	2.4	13.1
σ_{42}	0.4	0.75
Pelvis		
P_{52}, 10^{-5} cm/s	1	15
Loop geometry		
$\rho_1 := \gamma_1/1536$	$\frac{2}{3}$	1
$\rho_2 := \gamma_2/[1536(1-\rho_1)]$	0	1
$\rho_3 := \gamma_3/[1536(1-\rho_1)(1-\rho_2)]$	0	1

For the numerical solution of this inverse problem a partition with 14 subintervals and splines of degree $\leqslant 3$ are chosen (cf. Section 3). Thus, the discrete nonlinear-programming problem of Equations (48)–(53) consists of 100 independent variables, 84 nonlinear equality constraints, 4 nonlinear inequality constraints, and 34 bounds.

Tables 4,5 and Figures 3–5 give the results of these computations. The bounds of Table 3 are repeated in Table 4 for the convenience of the reader. The computed optima for ρ_1,ρ_2,ρ_3 corresponded to $\gamma_1 = 1024$, $\gamma_2 = 356$, $\gamma_3 = 0$, $\gamma_4 = 156$. Both the computed salt concentration in the central core (Figure 3) and the computed urea concentration in the central core (Figure

TABLE 4

COMPUTED OPTIMA FOR THE VARIABLE PARAMETERS IN THE BASE CASE

Parameter (for units see Table 3)	Lower bound	Computed optimum	Upper bound
Maximum rates of active transport			
Vm_{21}	0	14.76	44
Vm_{31}	0	8.82	44
Descending limb of Henle's loop			
Lp_1	5	Upper bound	252
P_{11}	0	Lower bound	47
P_{12}	0	Lower bound	20
σ_{11}	0.36	0.93	1
σ_{12}	0.4	Upper bound	1
Outer medullary collecting duct			
Lp_4	23	Upper bound	48.4
σ_{42}	0.4	Upper bound	1
Inner medullary collecting duct			
Lp_4	7.37	14.40	92
P_{42}	2.4	Lower bound	13.1
σ_{42}	0.4	Lower bound	0.75
Pelvis			
P_{52}	1	Upper bound	15
Loop geometry			
ρ_1	$\frac{2}{3}$	Lower bound	1
ρ_2	0	0.695	1
ρ_3	0	Lower bound	1

TABLE 5

COMPUTED TUBULE FLUID-TO-PLASMA RATIO FOR THE INULIN CONCENTRATION (BASE CASE)[a]

	Ratio								
s	DLH1	ALH1	DLH2	ALH2	DLH3	ALH3	DLH4	ALH4	CD
0	3	8.77	3	9.55	—	—	3	20.83	36.22
1.5	3.90	8.77	3.90	9.55	—	—	3.90	20.83	51.09
4.5	8.77	8.77	8.77	9.55	—	—	8.77	20.83	114.50
6.0			9.55	9.55	—	—	9.55	20.83	158.19
8.25					—	—	13.67	20.83	277.53
10.5							20.83	20.83	400

[a]DLHj (ALHj), descending (ascending) limb of Henle's loop of length b_j; CD, collecting duct.
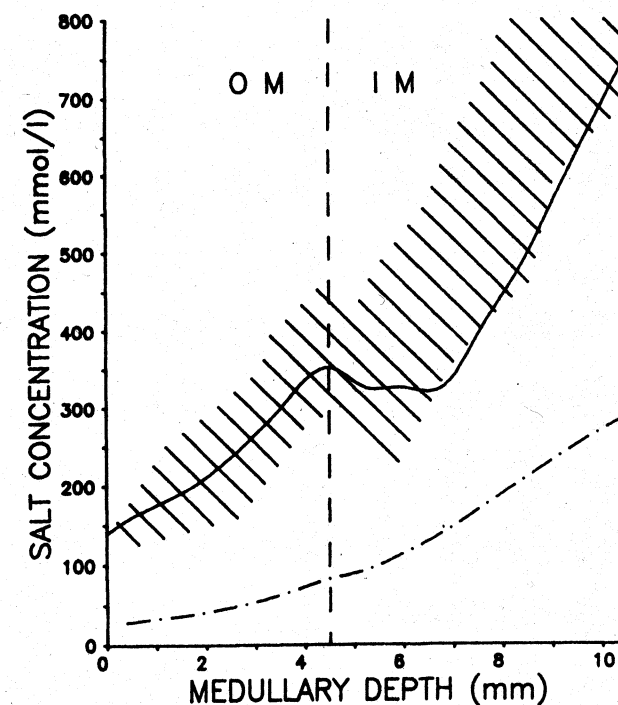

FIG. 3. Computed salt concentration for the base case in the central core (—) and in the collecting duct (–·–·); for comparison also measured slice concentrations [37] are given (hatched area); OM (IM), outer (inner) medulla.

4) are in satisfactory agreement with slice concentration measurements. The increase of the osmolarity in the inner medullary central core is moderately strong (Figure 5). Note that this is the objective function (38). Thus, the present model cannot explain stronger increases of inner medullary concentrations.

Some comments on the computed optima of the variable parameters in Table 4 seem in place: The second group of parameters in this table is related to the descending limbs of Henle's loops (DLH). The computed optima for these parameters demonstrate that the water recycling mode of DLH equilibration is most effective. This confirms the direct parameter
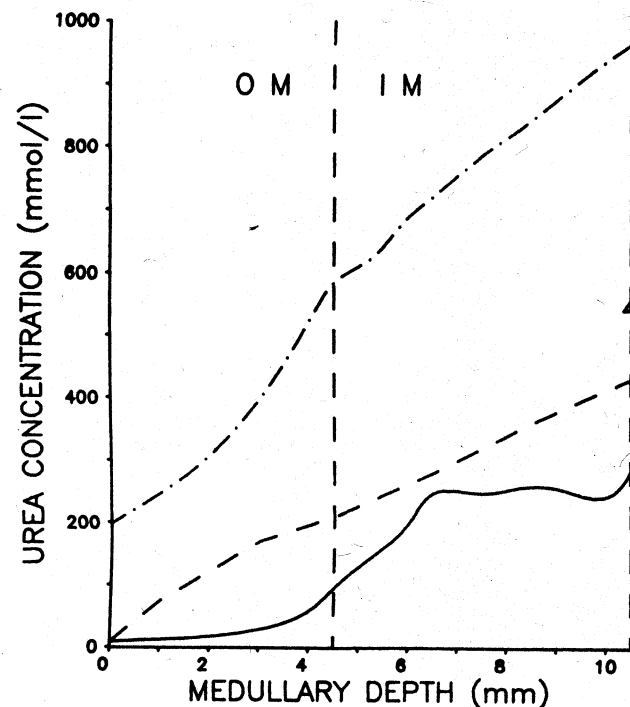
FIG. 4. Computed urea concentration for the base case in the central core (—), in the collecting duct (—·—·), and in the pelvis (Δ); for comparison also measured slice concentrations [57] are given (— — —); OM (IM), outer (inner) medulla.

FIG. 5. Computed osmolarity for the base case in the central core (—) and in the collecting duct (—·—·); OM (IM), outer (inner) medulla.

study in [7]. The computed optima for the last group of parameters in Table 4 show that a decreasing loop-of-Henle population as a function of increasing medullary depth is an important factor in the concentrating mechanism. The concentration capability of the present model is well above that of an otherwise similar model with only a single type of nephrons (see [55]). This is consistent with the direct parameter studies in [16, 58, 59].

The computed optimum for the urea permeability of the wall separating the pelvis and the papillary central core (P_{52}) allows a rather large amount of pelvic urea reflux. This together with the low urea permeability of the inner medullary collecting duct has a "delay effect" (cf. [4]): The entry of a high percentage of the inner medullary collecting duct urea load into the central core is delayed to the innermost depths of the medulla. This supports urea trapping in the inner medullary central core, which is a decisive feature for the passive concentration mechanism [2, 11].
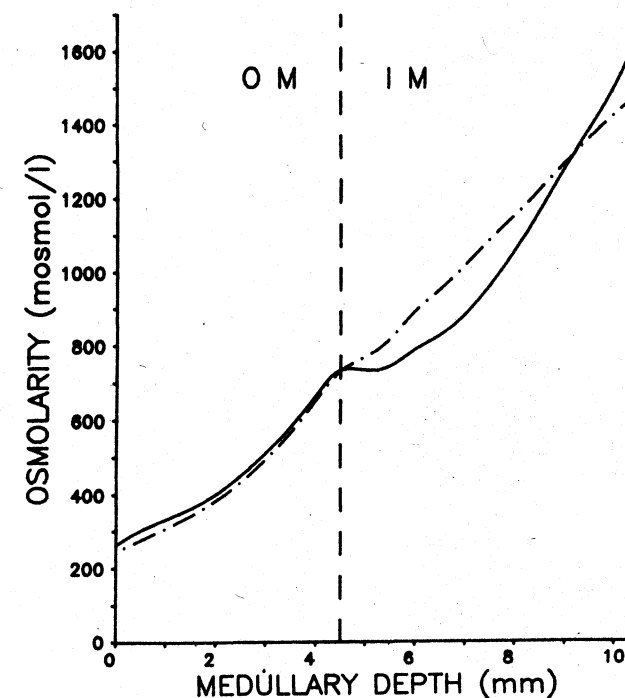
However, in a recent study [56] such urea reentry from the pelvis has been judged to be insignificant under normal steady-state conditions. Moreover, the corresponding permeability in the rabbit was measured to be an order of magnitude smaller than the computed optimum for P_{52} in Table 4. For a nonrabbit species, similar results have been reported in [60].

A delay effect (see above) is not necessarily restricted to the presence of pelvic urea reflux. Recent experiments [56], which have been inspired by mathematical modeling studies in [18], demonstrate a remarkable heterogeneity with respect to urea permeability of the inner medullary collecting duct. The urea permeability in the innermost part of the inner medullary collecting is found to be significantly higher than that in the outer third of this tubular segment. Obviously, this pattern allows a delay effect, too.

In order to study the functional implications of this heterogeneity by the inverse approach, the inner medullary collecting duct is subdivided into three parts. In the outermost part ($4.5 \leqslant s \leqslant 6.5$), the urea permeability (P_{42},

10^{-5} cm/s) is allowed to vary between the bounds 1.1 [56] and 2.4 [61]. In the innermost part ($8.25 \leqslant s \leqslant 10.5$), the corresponding bounds are 2.4 [61] and 14.9 [56]. The interval $6.5 \leqslant s \leqslant 8.25$ is modeled as a linear transition zone for P_{42}. The upper bound for P_{52} is an order of magnitude smaller than that in the base case [56]. The other bounds for the variable parameters are the same as in the base case (Table 3). The fixed parameters (Table 2), the inequality constraints (40)–(43), and the objective function (38) are identical

TABLE 6
COMPUTED OPTIMA FOR THE VARIABLE PARAMETERS
IN THE HETEROGENEOUS COLLECTING-DUCT CASE

Parameter (for units see Table 3)	Lower bound	Computed optimum	upper bound
Maximum rates of active transport			
Vm_{21}	0	16.84	44
Vm_{31}	0	5.70	44
Descending limb of Henle's loop			
Lp_1	5	Upper bound	252
P_{11}	0	Lower bound	47
P_{12}	0	Lower bound	20
σ_{11}	0.36	0.74	1
σ_{12}	0.4	Upper bound	1
Outer medullary collecting duct			
Lp_4	23	Upper bound	48.4
σ_{42}	0.4	0.85	1
Inner medullary collecting duct			
Lp_4	7.37	12.90	92
P_{42}: $4.5 \leqslant s \leqslant 6.5$	1.1	Lower bound	2.4
$\phantom{P_{42}:}8.25 \leqslant s \leqslant 10.5$	2.4	12.31	14.9
σ_{42}	0.4	Lower bound	0.75
Pelvis			
P_{52}	1	Upper bound	1.5
Loop geometry			
ρ_1	$\frac{2}{3}$	0.78	1
ρ_2	0	0.64	1
ρ_3	0	Lower bound	1

TABLE 7
COMPUTED TUBULE FLUID-TO-PLASMA RATIO FOR THE INULIN CONCENTRATION
(HETEROGENEOUS COLLECTING-DUCT CASE)[a]

	Ratio								
s	DLH1	ALH1	DLH2	ALH2	DLH3	ALH3	DLH4	ALH4	CD
0	3	11.37	3	14.05	—	—	3	22.48	38.64
1.5	3.76	11.37	3.76	14.05	—	—	3.76	22.48	59.14
4.5	11.37	11.37	11.37	14.05	—	—	11.37	22.48	142.32
6.0			14.05	14.05	—	—	14.05	22.48	208.78
8.25					—	—	20.20	22.48	320.14
10.5							22.48	22.48	400

[a] DLHj (ALHj), descending (ascending) limb of Henle's loop of length b_j; CD, collecting duct.
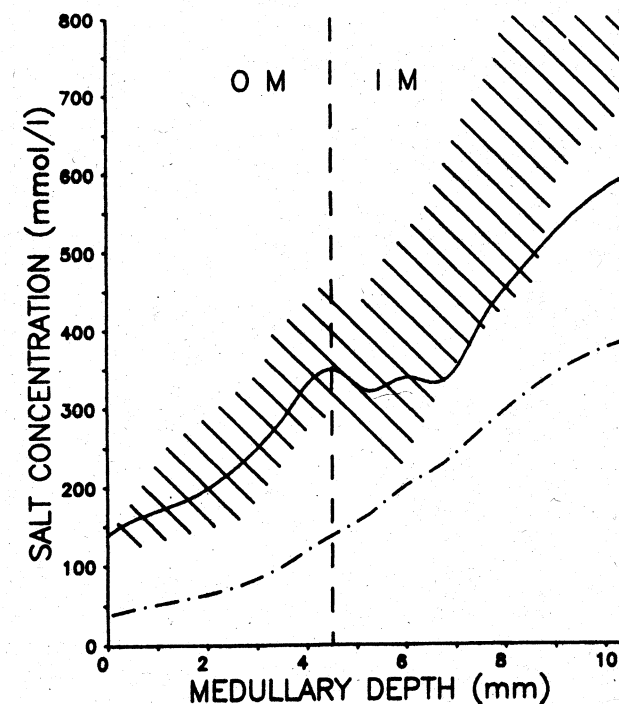

FIG. 6. Computed salt concentration for the heterogeneous collecting-duct case in the central core (—) and in the collecting duct (–·–·); for comparison also measured slice concentrations [37] are given (hatched area); OM (IM) outer (inner) medulla.
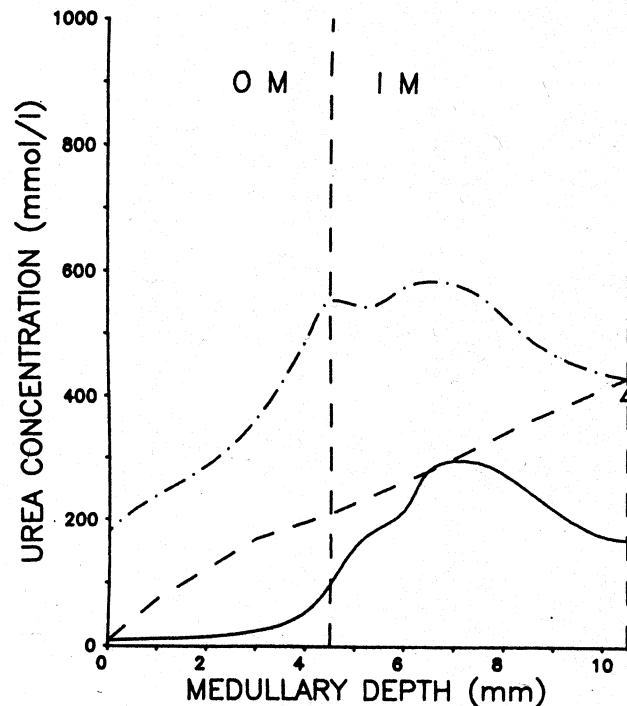
FIG. 7. Computed urea concentration for the heterogeneous collecting-duct case in the central core (—), in the collecting duct (−·−·), and in the pelvis (△); for comparison also measured slice concentrations [57] are given (− − −); OM (IM), outer (inner) medulla.

FIG. 8. Computed osmolarity for the heterogeneous collecting-duct case in the central core (—) and in the collecting duct (−·−·); OM (IM), outer (inner) medulla.

to those of the base case as well. In the following, this inverse problem will be referred to as the heterogeneous collecting-duct case.

Tables 6,7 and Figures 6–8 give the results of these computations. The computed optima for ρ_1, ρ_2, ρ_3 correspond to $\gamma_1 = 1195$, $\gamma_2 = 217$, $\gamma_3 = 0$, $\gamma_4 = 124$. The computed optima for P_{42} are in accord with the delay effect suggested in [56]. Because of the optimal selection of the variable parameters by the inverse approach, the computed increase of the osmolarity in the inner medullary central core (cf. Figure 8) is considerably stronger than the corresponding increase in the simulations of [18]. Note that the latter simulations also model inner medullary collecting duct heterogeneity. Nethertheless, a comparison of Figures 6–8 with Figures 3–5 reveals that the delay effect produced by the collecting duct heterogeneity is less efficient than the corresponding delay effect in the base case, which is due to pelvic urea reflux.
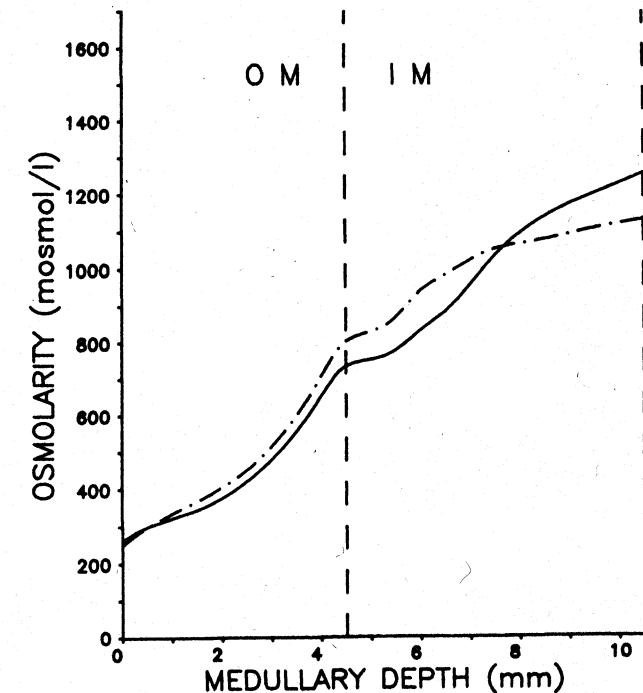
5. DISCUSSION

The inverse approach presented in Sections 2–4 allows rigorous judgement of the potential of a given kidney modeling technique by determining the optimal inner medullary concentration increase. Note that the central core is an idealization that does not take into account the possible dissipative losses due to the system of the vasa recta (see [1]). Thus, the computed optimal inner medullary concentration increases of the present paper are upper bounds for those increases that would be predicted by a model that includes the vasa recta as separate structures. In spite of this idealization, the results of the base case are consistent only with the flattest measured inner medullary concentration profiles (cf. Figures 3, 4). If the pelvic urea reflux is restricted according to recent measurements (heterogeneous collecting-duct case), the agreement is not satisfactory (cf. Figures 6, 7). However, the situation improves drastically, if a "salt transport cascade" [19, 62] is included

in the model. Such a transport cascade occurs if the upper parts of the long descending limbs of Henle's loops are able to secrete salt actively into the tubular fluid. This feature has been included in a model which is otherwise similar to that given here [19]. For this model, the inverse approach was able to determine a parameter set which predicts a very strong concentration increase over the inner medullary central core (osmolarity at the inner outer medullary junction $s = 4.5$: 976 mosmol/l; at the papillary tip, $s = 10.5$: 4343 mosmol/l; see [55]).

At present, the assumption of active salt transport into certain parts of the descending limbs of Henle's loops is backed only by morphological observations and lacks experimental evidence. However, it has been pointed out recently [63] that a salt transport cascade is not necessarily restricted to the presence of active salt transport into the descending limbs and could operate on the basis of the complementary processes of cycles and separations as well. A verification of this suggestion requires further modeling efforts.

REFERENCES

1 A. S. Wexler, R. E. Kalaba, and D. J. Marsh, Passive, one-dimensional countercurrent models do not simulate hypertonic urine formation, *Amer. J. Physiol.* 253 (*Renal Fluid Electrolyte Physiol.* 22):F1020–F1030 (1987).

2 J. L. Stephenson, Concentration of urine in a central core model of the renal counterflow system, *Kidney Internat.* 2:85–94 (1972).

3 R. B. Kellogg, Some Singular Perturbation Problems in Renal Models, Manuscript, Univ. of Maryland, College Park, Md., 1988.

4 P. Lory, A. Gilg, and M. Horster, Renal countercurent system: Role of collecting duct convergence and pelvic urea predicted from a mathematical model, *J. Math. Biol.* 16:281–304 (1983).

5 W. Kriz, Structural organization of the renal medulla: Comparative and functional aspects, *Amer. J. Physiol.* 241 (*Regulatory Integrative Comp. Physiol.* 10):R3–R26 (1981).

6 A. Katchalsky and P. F. Curran, *Nonequilibrium Thermodynamics in Biophysics*, Harvard U.P., Cambridge, Mass., 1967.

7 L. C. Moore and D. J. Marsh, How descending limb of Henle's loop permeability affects hypertonic urine formation, *Amer. J. Physiol.* 239 (*Renal Fluid Electrolyte Physiol.* 8):F57–F71 (1980).

8 A. Gilg, Simulationen an einem zeitabhängigen Modell des Gegenstromsystems der Niere, in *Simulationstechnik*, Informatik-Fachber. 109 (D. F. P. Möller, Ed.), Springer-Verlag, Berlin, 1985.

9 A. Rocha and J. P. Kokko, Sodium chloride and water transport in the medullary thick ascending limb of Henle, *J. Clinical Investigation* 52:612–623 (1973).

10 M. Imai and J. P. Kokko, Sodium chloride, urea and water transport in the thin ascending limb of Henle: Generation of osmotic gradients by passive diffusion of solutes, *J. Clinical Investigation* 53:393–402 (1974).

11 J. P. Kokko and F. C. Rector, Countercurrent multiplication system without active transport in inner medulla, *Kidney Internat.* 2:214–223 (1972).

12 J. L. Stephenson, R. P. Tewarson, and R. Mejia, Quantitative analysis of mass and energy balance in non-ideal models of the renal counterflow system, *Proc. Nat. Acad. Sci. U.S.A.* 71:1618–1622 (1974).

13 J. L. Stephenson, R. Mejia, and R. P. Tewarson, Model of solute and water movement in the kidney, *Proc. Nat. Acad. Sci. U.S.A.* 73:252–256 (1976).

14 R. Mejia and J. L. Stephenson, Numerical solution of multinephron kidney equations, *J. Comput. Phys.* 32:325–246 (1979).

15 L. C. Moore, D. J. Marsh, and C. M. Martin, Loop of Henle during the water-to-antidiuresis transition in Brattleboro rats, *Amer. J. Physiol.* 239 (*Renal Fluid Electrolyte Physiol.* 8):F72–F83 (1980).

16 R. Mejia and J. L. Stephenson, Solution of multinephron, multisolute model of the mammalian kidney by Newton and continuation methods, *Math. Biosci.* 68:279–298 (1984).

17 M. Horster, A. Gilg, and P. Lory, Determinants of axial osmotic gradients in the differentiating countercurrent system, *Amer. J. Physiol.* 246 (*Renal Fluid Electrolyte Physiol.* 15):F124–F132 (1984).

18 P. S. Chandhoke, G. M. Saidel, and M. A. Knepper, Role of inner medullary collecting duct NaCl transport in urinary concentration, *Amer. J. Physiol.* 249 (*Renal Fluid Electrolyte Physiol.* 18):F688–F697 (1985).

19 P. Lory, Effectiveness of a salt transport cascade in the renal medulla: Computer simulations, *Amer. J. Physiol.* 252 (*Renal Fluid Electrolyte Physiol.* 21):F1095–F1102 (1987).

20 J. L. Stephenson, Y. Zhang, A Eftekhari, and R. Tewarson, Electrolyte transport in a central core model of the renal medulla, *Amer. J. Physiol.* 253 (*Renal Fluid Electrolyte Physiol.* 22):F982–F997 (1987).

21 R. Mejia, R. B. Kellogg, and J. L. Stephenson, Comparison of numerical methods for renal network flows, *J. Comput. Phys.* 23:53–62 (1977).

22 R. P. Tewarson and S. Gupta, A sparse matrix method for renal models, *Math. Biosci.* 61:191–203 (1982).

23 R. P. Tewarson, J. L. Stephenson, M. Garcia, and Y. Zhang, On the solution of equations for renal counterflow models, *Comput. Biol. and Med.* 15:287–295 (1985).

24 R. E. Bellman and R. E. Kalaba, *Quasilinearization and Nonlinear Boundary Value Problems*, Elsevier, New York, 1965.

25 A. S. Wexler, R. E. Kalaba, and D. J. Marsh, Automatic derivative evaluation in solving boundary value problems: The renal medulla, *Amer. J. Physiol.* 251 (*Renal Fluid Electrolyte Physiol.* 20):F358–F378 (1986).

26 A. Wexler, Solution of nonlinear boundary value problems coupled to a system of algebraic equations using quasilinearization, *Nonlinear Anal.* 11:691–696 (1987).

27 R. E. Kalaba and A. S. Wexler, New methods for boundary value problems, *Math. Comput. Modelling* 11:855–857 (1988).

28 M. R. Scott, *Invariant Imbedding and its Applications to Ordinary Differential Equations*, Addison-Wesley, Reading Mass., 1973.

29 J. Casti and R. Kalaba, *Imbedding Methods in Applied Mathematics*, Addison-Wesley, Reading, Mass., 1973.

30 J. Buell, R. Kalaba, and D. Marsh, On a boundary value problem in the theory of urine formation, *Appl. Math. Comput.* 5:55–67 (1979).

31 A. S. Wexler, R. E. Kalaba, L. S. Tesfatsion, and D. J. Marsh, An invariant-imbedding solution of general linear two-point boundary-value problems, *Appl. Math. Comput.* 26:237–244 (1988).

32 J. Stoer and R. Bulirsch, *Introduction to Numerical Analysis*, Springer-Verlag, New York, 1980.

33 P. Lory, Ein Semi-Kollokationsverfahren zur numerischen Lösung von Nierenmodellen, Report TUM-M8501, Technische Univ. München, Mathematisches Institut, München, West Germany, 1985.

34 C. de Boor and B. Swartz, Collocation at Gaussian points, *SIAM J. Numer. Anal.* 10:582–606 (1973).

35 C. W. Gottschalk and M. Mylle, Micropuncture study of the mammalian urinary concentrating mechanism: Evidence for the countercurrent hypothesis, *Amer. J. Physiol.* 196:927–936 (1959).

36 R. E. Oliver, D. R. Roy, and R. L. Jamison, Urinary concentration in the papillary collecting duct of the rat, *J. Clinical Investigation* 69:157–164 (1982).

37 H. Koepsell, W. A. P. Nicholson, W. Kriz, and H. J. Höhling, Measurements of exponential gradients of sodium and chlorine in the rat kidney medulla using the electron microprobe, *Pfluegers Arch.* 350:167–184 (1974).

38 C. de Boor, *A Practical Guide to Splines*, Springer-Verlag, New York, 1978.

39 R. Bulirsch and J. Stoer, Numerical treatment of ordinary differential equations by extrapolation methods, *Numer. Math.* 8:1–13 (1966).

40 W. B. Gragg, On extrapolation algorithms for ordinary initial value problems, *SIAM J. Numer. Anal.* 2:384–403 (1965).

41 H. G. Hussels, Schrittweitensteuerung bei der Integration gewöhnlicher Differentialgleichungen mit Extrapolationsverfahren, Diplomarbeit, Univ. Köln, mathematisches Inst., Köln, West Germany, 1973.

42 E. Fehlberg, Klassische Runge-Kutta Formeln fünfter und siebenter Ordnung mit Schrittweitenkontrolle, *Computing* 4:93–106 (1969).

43 C. W. Gear, *Numerical Initial Value Problems in Ordinary Differential Equations*, Prentice-Hall, Englewood Cliffs, N.J., 1971.

44 D. Kraft, A Software Package for Sequential Quadratic Programming, Report DFVLR-FB 88-28, Deutsche Foschungs- und Versuchsanstalt für Luft- und Raumfahrt, Oberpfaffenhofen, West Germany, 1988.

45 R. B. Wilson, A simplicial algorithm for concave programming, Ph.D. Thesis, Graduate School of Business Administration, Harvard Univ., Cambridge, Mass., 1963.

46 S.-P. Han, A globally convergent method for nonlinear programming, *J. Optim. Theory Appl.* 22:297–309 (1977).

47 M. J. D. Powell, A fast algorithm for nonlinearily constrained optimization calculations, in *Numerical Analysis, Proceedings of the Biennial Conference Held at Dundee, June 1977*, Lecture Notes in Math. 630 (G. A. Watson, Ed.), Springer-Verlag, Berlin, 1978.

48 M. J. D. Powell, The convergence of variable metric methods for nonlinearly constrained optimization calculations, in *Nonlinear Programming, No. 3* (O. L. Mangasarian, R. R. Meyer, and S. M. Robinson, Eds.), Academic, New York, 1978.

49 K. Schittkowski, The nonlinear programming method of Wilson, Han, and Powell with an augmented Lagrangian type line search function, Part 1: Convergence analysis, *Numer. Math.* 38:83–114 (1981).

50 K. Schittkowski, The nonlinear programming method of Wilson, Han, and Powell with an augmented Lagrangian type line search function, Part 2: An efficient implementation with linear least squares subproblems, *Numer. Math.* 38:115–127 (1981).

51 R. Fletcher, *Practical Methods of Optimization, Vol. 2, Constrained Optimization*, Wiley, Chichester, 1981.

52 K. Schittkowski, *Nonlinear Programming Codes. Information, Test, Performance*, Lecture Notes in Econom. and Math. Systems 183, Springer-Verlag, Berlin, 1980.

53 W. Hock and K. Schittkowski, *Test Examples for Nonlinear Programming Codes*, Lecture Notes in Econom. and Math. Systems 187, Springer-Verlag, Berlin, 1981.

54 C. L. Lawson and R. J. Hanson, *Solving Least Squares Problems*, Prentice-Hall, Englewood Cliffs, N.J., 1974.

55 M. Breinbauer, Das Nierenmodell als inverses Problem, Diplomarbeit, Technische Univ. München, Mathematisches Inst., München, West Germany, 1988.

56 J. M. Sands and M. A. Knepper, Urea permeability of mammalian inner medullary collecting duct system and papillary surface epithelium, *J. Clinical Investigation* 79:138–147 (1987).

57 R. A. Gunther and L. Rabinowitz, Urea and renal concentrating ability in the rabbit, *Kidney Internat.* 17:205–222 (1980).

58 H. E. Layton, Distribution of Henle's loops may enhance urine concentrating capability, *Biophysical J.* 49:1033–1040 (1986).

59 H. E. Layton, Urea transport in a distributed loop model of the urine concentrating mechanism, *Amer. J. Physiol.* 258 (*Renal Fluid Electrolyte Physiol.* 27):F1110–F1124 (1990).

60 D. J. Marsh and C. M. Martin, Lack of water or urea movement from pelvic urine to papilla in hydropenic hamsters, *Mineral and Electrolyte Metabolism* 3:81–86 (1980).

61 A. Rocha and J. P. Kokko, Permeability of medullary nephron segments to urea and water: Effect of vasopressin, *Kidney Internat.* 6:379–387 (1974).

62 W. Kriz, Structural organization of the renal medullary counterflow system, *Fed. Proc.* 42:2379–2385 (1983).

63 K. V. Lemley and W. Kriz, Cycles and separations: The histotopography of the urinary concentrating process, *Kidney Internat.* 31:538–548 (1987).